

Facets Matching of Platinum and Ferric Oxide in Highly Efficient Catalyst Design for Low-Temperature CO Oxidation

Yanling Ma, Fan Li, Xiaobo Ren, Wenlong Chen, Chao Li, Peng Tao, Chengyi Song, Wen Shang, Rong Huang, Baoliang Lv, Hong Zhu, Tao Deng, and Jianbo Wu

ACS Appl. Mater. Interfaces, **Just Accepted Manuscript** • DOI: 10.1021/acsami.8b03579 • Publication Date (Web): 04 Apr 2018

Downloaded from <http://pubs.acs.org> on April 16, 2018

Just Accepted

“Just Accepted” manuscripts have been peer-reviewed and accepted for publication. They are posted online prior to technical editing, formatting for publication and author proofing. The American Chemical Society provides “Just Accepted” as a service to the research community to expedite the dissemination of scientific material as soon as possible after acceptance. “Just Accepted” manuscripts appear in full in PDF format accompanied by an HTML abstract. “Just Accepted” manuscripts have been fully peer reviewed, but should not be considered the official version of record. They are citable by the Digital Object Identifier (DOI®). “Just Accepted” is an optional service offered to authors. Therefore, the “Just Accepted” Web site may not include all articles that will be published in the journal. After a manuscript is technically edited and formatted, it will be removed from the “Just Accepted” Web site and published as an ASAP article. Note that technical editing may introduce minor changes to the manuscript text and/or graphics which could affect content, and all legal disclaimers and ethical guidelines that apply to the journal pertain. ACS cannot be held responsible for errors or consequences arising from the use of information contained in these “Just Accepted” manuscripts.

Facets Matching of Platinum and Ferric Oxide in Highly Efficient Catalyst Design for Low- Temperature CO Oxidation

*Yanling Ma^{1, ‡}, Fan Li^{1, ‡}, Xiaobo Ren^{2, 3, ‡}, Wenlong Chen¹, Chao Li⁴, Peng Tao¹, Chengyi Song¹,
Wen Shang¹, Rong Huang^{*, 4}, Baoliang Lv^{*, 2}, Hong Zhu^{*, 1, 5, 6}, Tao Deng¹, Jianbo Wu^{*, 1, 6}*

¹State Key Laboratory of Metal Matrix Composites, School of Materials Science and Engineering, Shanghai Jiao Tong University, 800 Dongchuan Road, Shanghai, 200240, P. R. China.

²State Key Laboratory of Coal Conversion, Institute of Coal Chemistry, Chinese Academy of Sciences, Taiyuan, 030001, P. R. China.

³University of Chinese Academy of Sciences, Beijing, 100049, P. R. China.

⁴Key Laboratory of Polar Materials and Devices, Ministry of Education, East China Normal University, Shanghai, 200241, P. R. China.

⁵University of Michigan – Shanghai Jiao Tong University Joint Institute, Shanghai Jiao Tong University, 800 Dongchuan Road, Shanghai, 200240, P. R. China.

1
2
3 ⁶Materials Genome Initiative Center, Shanghai Jiao Tong University, 800 Dongchuan Road,
4
5 Shanghai, 200240, P. R. China.
6
7

8
9 KEYWORDS: heterogeneous catalysis, CO oxidation, facets matching, catalyst design, surface
10
11 adsorption
12
13

14
15 ABSTRACT
16
17

18
19 Rational design of supported noble metal is of great importance for highly efficient
20
21 heterogeneous catalysts. Based on the distinct adsorption characteristics of noble metal and
22
23 transition metal oxides towards O₂ and CO, the overall catalytic performance of CO oxidation
24
25 reaction could be further modified by controlling the materials surface property to achieve
26
27 optimal adsorption activity. Here we studied the influence of facets matching between both
28
29 platinum and ferric oxide support on CO conversion efficiency. It shows that the activity of four
30
31 catalysts ranks following the order of Pt {100}/ α -Fe₂O₃ {104} > Pt {100}/ α -Fe₂O₃ {001} > Pt
32
33 {111}/ α -Fe₂O₃ {001} > Pt {111}/ α -Fe₂O₃ {104}. The Strong Metal-Support Interaction (SMSI)
34
35 and adsorption energy varying with matched enclosed surface are demonstrated by density
36
37 functional theory (DFT) based on the projected d-band density of states (DOS). Compared with
38
39 the other three cases, the combination of Pt {100} and α -Fe₂O₃ {104} successfully weakens CO
40
41 poisoning and provides proper active sites for O₂ adsorption. It reveals that the facets matching
42
43 could be a practicable approach to design catalysts with enhanced catalytic performance.
44
45
46
47
48
49
50
51
52
53
54
55
56
57
58
59
60

1. INTRODUCTION

Supported noble-metal continues to be one of the most critical heterogeneous catalysts towards many significant chemical reactions in industrial production.¹⁻³ The Strong Metal-Support Interaction (SMSI) is regarded to play an important role in modifying the complementary adsorption, providing catalytic active sites, and modulating electronic structure.⁴⁻⁸ For instance, metal-on-oxide has been widely used as a promising candidate among thermal catalysts especially for CO oxidation—a typical reaction that strongly depends on the intrinsic properties of metal nanoparticles (NPs) and oxides supports.^{1, 4, 9-11} Therefore, the rational design could provide a significant approach to highly efficient catalysts.¹²⁻¹⁵

Generally, it has been demonstrated that the catalytic activity of supported noble-metal catalysts could be greatly influenced by multiple factors including the size of metal NPs, composition or crystal phase of support.^{4, 16} Such as the single atom catalysts with both low loading of noble metal and high active surface exhibit remarkable performance towards heterogeneous catalysis but the stability under thermal treatment and tendency to aggregation are still questionable.¹⁷⁻¹⁹ Besides, even the same composition with different crystal phases could show distinct activity as well.²⁰ For example, Au/ γ -Fe₂O₃ catalyst becomes more efficient than Au/ α -Fe₂O₃ towards CO oxidation owing to the higher redox property originated from reverse spinel structure.¹

Furthermore, the Au NPs/CeO₂ dominated with {110} and {100} facets has been reported to possess improved performance to water-gas shift reaction compared with CeO₂ terminated by other surfaces.²¹ Consequently, the exposed crystal facets of both the supported noble-metal and oxides also determine the surface properties including thermodynamic stability and interfacial adsorption of catalysts which is closely related to the catalytic activity.²¹⁻²⁴ Even though the

1
2
3 intriguing facet-dependence of thermal catalytic reactions has aroused wide discussion, most
4 recent studies focus on the self-governed effect of noble metal NPs or supports with different
5 exposed surfaces instead of the coordination between both.^{4, 21, 25} However, according to the
6
7 Langmuir-Hinshelwood (L-H) mechanism of CO oxidation that has been widely accepted, the
8 noble metal NPs and oxides support display different characteristic adsorption properties towards
9
10 CO oxidation reaction and then simultaneously modify the overall performance.^{9, 26, 27} Typically,
11 the active sites on noble metal surface are predominately occupied by CO molecules which
12 blocks the adsorption of O₂ when the oxides supports are inert and hence leads to the competitive
13 adsorption and poor activity under low temperature; while more active adsorption sites for O₂
14 provided by reducible oxides successfully weaken the CO poisonous effect thus exhibit enhanced
15 performance.⁹ Based on the classic theory of adsorbate-surface interaction, the adsorption
16 properties is mainly determined by electronic structure (energy band, density of state) and
17 surface structure such as atomic arrangement of the materials surface so the adsorption energy of
18 both CO and O₂ is possible to be modified with optimal activated adsorbate to participate in
19 reaction.^{28, 29} Taking the facets matching between noble metal NPs and oxide supports into
20 consideration, it is prone to provide a novel point of view for catalyst design and the SMSI
21 varying with exposed surface could be observed experimentally.

22
23
24
25
26
27
28
29
30
31
32
33
34
35
36
37
38
39
40
41
42 Herein, we demonstrate the obvious facet matching dependence of Pt/ α -Fe₂O₃ catalysts toward
43 CO oxidation reaction. Pt NPs without well-defined morphology thereby analyzed as Wulff
44 structure (denoted as Pt {111} for simplification) and Pt nanocubes (Pt NCs, denoted as Pt
45 {100}) supported by α -Fe₂O₃ nanosheets (NSs) with exposed surface {001} (denoted as Fe₂O₃
46 {001}) and α -Fe₂O₃ rhombohedra (Rhomb) with exposed surface {104} (denoted as Fe₂O₃
47 {104}), respectively, are fabricated based on a modified CO-assisted gas phase synthetic
48
49
50
51
52
53
54
55
56
57
58
59
60

1
2
3 method.^{30, 31, 32} It shows that the four combinations exhibit different catalytic activity following
4 the order of Pt {100}/Fe₂O₃ {104} > Pt {100}/Fe₂O₃ {001} > Pt {111}/Fe₂O₃ {001} > Pt
5 {111}/Fe₂O₃ {104}. The Pt {100}/Fe₂O₃ {104} catalyst turns out to be the most active with the
6 lowest temperature around 60 °C to achieve 100% CO conversion efficiency. Additionally,
7 density functional theory (DFT) calculation is performed to further understand the relation
8 between catalytic activity, adsorption energy of CO and O₂ on surface of Pt and Fe₂O₃ and the
9 overall reaction Gibbs energy among the target four cases.
10
11
12
13
14
15
16
17
18

19 2. RESULTS AND DISCUSSION

20
21 **2.1. Synthesis and Characterization of the Catalyst.** Different morphology of Fe₂O₃
22 including NSs and Rhomb were pre-synthesized by hydrothermal method.^{33, 34} Figure S1a, b, d, e
23 shows the corresponding scanning electron microscope (SEM) images and both present uniform
24 shape and size. After being loaded to the Fe₂O₃ support, the Pt precursors underwent
25 programmed annealing in CO atmosphere to obtain the supported Pt cluster catalysts. The
26 exposed surfaces of Pt cluster were controlled by the addition of oleylamine (OAm) as capping
27 agent.³⁰ Low-magnification transition electron microscope (TEM) characterization of the
28 synthesized Pt/Fe₂O₃ catalysts is shown in Figure S2. It exhibits that the small Pt NPs around
29 size of 4 nm without specific morphology and Pt NCs with slightly larger size and sharp edges
30 were loaded apart on the Fe₂O₃ NSs and Fe₂O₃ Rhombs. Figure S3 is the size distribution of Pt
31 nanoclusters under these four cases. Even though the single Pt NP seemed smaller than Pt NC,
32 the majority of the Pt NPs were inclined to gather around thus forming larger groups. Therefore,
33 the influence resulting from size of Pt clusters could be eliminated. The powder X-ray diffraction
34 (PXRD) patterns (Figure S4) of the four samples all present the characteristic diffraction peaks
35 of α -Fe₂O₃ phase without any signal of Pt due to the small particle size and low loading of Pt.⁴
36
37
38
39
40
41
42
43
44
45
46
47
48
49
50
51
52
53
54
55
56
57
58
59
60

1
2
3 Low-magnification TEM images of the four samples after low temperature CO oxidation test
4 (Figure S5) appears slight trend of aggregation, however, most Pt nanocubes exhibited better
5 shape preservation with sharp edges. High-resolution TEM images in Figure 1 reveal the
6 different facets matching between Pt cluster and α -Fe₂O₃. As for Pt clusters, the NCs in Figure 1a
7 and 1b show the lattice fringes with d-spacing of 0.196 nm and 0.190 nm respectively,
8 demonstrating the enclosed facets belonging to {100} planes of face-centered cubic (fcc) Pt; the
9 NPs in Figure 1c and 1d show the lattice fringes with d-spacing of 0.227 nm and 0.226 nm
10 respectively, corresponding to the {111} planes of fcc Pt. For α -Fe₂O₃ supports, the lattice
11 fringes in two crystal orientations with both d-spacing of 0.249 nm in Figure 1b and Figure S1c
12 forming the angle around 120° indicates that the facets parallel to the projection belong to {001}
13 plane of α -Fe₂O₃.³³ Similarly, the lattice fringes with d-spacing of 0.268 nm in Figure 1d and
14 Figure S1f reveals the enclosed {104} planes of α -Fe₂O₃.³⁴ The inset at each upper right corner
15 shows the corresponding atomic model illustrations towards four configurations. The Pt NPs
16 were represented by classic Wulff structure with selected Pt {111} as the contiguous plane with
17 Fe₂O₃ support cleaved with {001} or {104} surface and the Pt {100} for Pt NCs.

18
19
20
21
22
23
24
25
26
27
28
29
30
31
32
33
34
35
36
37
38 **2.2. CO Oxidation Catalytic Activity.** As for as it is concerned, both noble metal NPs and
39 Fe₂O₃ as promoted oxides support play critical but well-divided roles in CO oxidation process
40 according to the distinct adsorption properties towards CO and O₂. Preferential adsorption and
41 activation of CO on surface of Pt and O₂ on Fe₂O₃ coordinately influence the catalytic activity.^{9,}
42
43
44
45
46
47
48
49
50
51
52
53
54
55
56
57
58
59
60
61
62
63
64
65
66
67
68
69
70
71
72
73
74
75
76
77
78
79
80
81
82
83
84
85
86
87
88
89
90
91
92
93
94
95
96
97
98
99
100
101
102
103
104
105
106
107
108
109
110
111
112
113
114
115
116
117
118
119
120
121
122
123
124
125
126
127
128
129
130
131
132
133
134
135
136
137
138
139
140
141
142
143
144
145
146
147
148
149
150
151
152
153
154
155
156
157
158
159
160
161
162
163
164
165
166
167
168
169
170
171
172
173
174
175
176
177
178
179
180
181
182
183
184
185
186
187
188
189
190
191
192
193
194
195
196
197
198
199
200
201
202
203
204
205
206
207
208
209
210
211
212
213
214
215
216
217
218
219
220
221
222
223
224
225
226
227
228
229
230
231
232
233
234
235
236
237
238
239
240
241
242
243
244
245
246
247
248
249
250
251
252
253
254
255
256
257
258
259
260
261
262
263
264
265
266
267
268
269
270
271
272
273
274
275
276
277
278
279
280
281
282
283
284
285
286
287
288
289
290
291
292
293
294
295
296
297
298
299
300
301
302
303
304
305
306
307
308
309
310
311
312
313
314
315
316
317
318
319
320
321
322
323
324
325
326
327
328
329
330
331
332
333
334
335
336
337
338
339
340
341
342
343
344
345
346
347
348
349
350
351
352
353
354
355
356
357
358
359
360
361
362
363
364
365
366
367
368
369
370
371
372
373
374
375
376
377
378
379
380
381
382
383
384
385
386
387
388
389
390
391
392
393
394
395
396
397
398
399
400
401
402
403
404
405
406
407
408
409
410
411
412
413
414
415
416
417
418
419
420
421
422
423
424
425
426
427
428
429
430
431
432
433
434
435
436
437
438
439
440
441
442
443
444
445
446
447
448
449
450
451
452
453
454
455
456
457
458
459
460
461
462
463
464
465
466
467
468
469
470
471
472
473
474
475
476
477
478
479
480
481
482
483
484
485
486
487
488
489
490
491
492
493
494
495
496
497
498
499
500
501
502
503
504
505
506
507
508
509
510
511
512
513
514
515
516
517
518
519
520
521
522
523
524
525
526
527
528
529
530
531
532
533
534
535
536
537
538
539
540
541
542
543
544
545
546
547
548
549
550
551
552
553
554
555
556
557
558
559
560
561
562
563
564
565
566
567
568
569
570
571
572
573
574
575
576
577
578
579
580
581
582
583
584
585
586
587
588
589
590
591
592
593
594
595
596
597
598
599
600
601
602
603
604
605
606
607
608
609
610
611
612
613
614
615
616
617
618
619
620
621
622
623
624
625
626
627
628
629
630
631
632
633
634
635
636
637
638
639
640
641
642
643
644
645
646
647
648
649
650
651
652
653
654
655
656
657
658
659
660
661
662
663
664
665
666
667
668
669
670
671
672
673
674
675
676
677
678
679
680
681
682
683
684
685
686
687
688
689
690
691
692
693
694
695
696
697
698
699
700
701
702
703
704
705
706
707
708
709
710
711
712
713
714
715
716
717
718
719
720
721
722
723
724
725
726
727
728
729
730
731
732
733
734
735
736
737
738
739
740
741
742
743
744
745
746
747
748
749
750
751
752
753
754
755
756
757
758
759
760
761
762
763
764
765
766
767
768
769
770
771
772
773
774
775
776
777
778
779
780
781
782
783
784
785
786
787
788
789
790
791
792
793
794
795
796
797
798
799
800
801
802
803
804
805
806
807
808
809
810
811
812
813
814
815
816
817
818
819
820
821
822
823
824
825
826
827
828
829
830
831
832
833
834
835
836
837
838
839
840
841
842
843
844
845
846
847
848
849
850
851
852
853
854
855
856
857
858
859
860
861
862
863
864
865
866
867
868
869
870
871
872
873
874
875
876
877
878
879
880
881
882
883
884
885
886
887
888
889
890
891
892
893
894
895
896
897
898
899
900
901
902
903
904
905
906
907
908
909
910
911
912
913
914
915
916
917
918
919
920
921
922
923
924
925
926
927
928
929
930
931
932
933
934
935
936
937
938
939
940
941
942
943
944
945
946
947
948
949
950
951
952
953
954
955
956
957
958
959
960
961
962
963
964
965
966
967
968
969
970
971
972
973
974
975
976
977
978
979
980
981
982
983
984
985
986
987
988
989
990
991
992
993
994
995
996
997
998
999
1000

1
2
3 occurring on the gas-solid interface greatly differs from exposed facets, the modification of
4 overall active sites occupied by CO and O₂ via modest facets matching between Pt and Fe₂O₃
5 could possibly extricate the Pt surface from CO poison and achieve optimal efficiency.²⁹
6
7

8
9
10 The CO oxidation reaction was measured in a fixed-bed reactor system with a feeding gas
11 mixture composed of 1 vol% CO and 1 vol% O₂ balanced with N₂. The space velocity (SV) was
12 set as 18, 750 mL·h⁻¹·g⁻¹_{catalyst}. Preactivation under O₂/ N₂ (21 vol% / 79 vol %) at 250 °C for 60
13 min was conducted prior to the test. Figure 2 shows the comparison of CO conversion curves for
14 CO oxidation as a function of temperature on different facet matching catalysts. When the
15 supported Pt clusters are Pt NPs, the combination with α-Fe₂O₃ NSs exhibits higher activity than
16 α-Fe₂O₃ Rhomb towards CO oxidation reaction whereas both the lowest temperatures to reach
17 100% efficiency of CO conversion (T₁₀₀) still exceed 100 °C. Especially for the Pt NPs/α-Fe₂O₃
18 Rhomb, it maintained inactive between a wide temperature range (<120 °C). However, the
19 performance dramatically reversed along with remarkable enhancement after the supported Pt
20 clusters turned to Pt NCs indicating the non-negligible significance of exposed facet matching
21 between supported Pt cluster and α-Fe₂O₃. Compared with the Pt NPs/α-Fe₂O₃ system, α-Fe₂O₃
22 supported Pt NCs catalysts became much more active during low temperature range and the CO
23 could be totally oxidized at 60 °C and 80 °C severally by Pt NPs/α-Fe₂O₃ Rhomb and Pt NPs/α-
24 Fe₂O₃ NSs.
25
26
27
28
29
30
31
32
33
34
35
36
37
38
39
40
41
42
43

44 The specific rate at 60 °C was measured according to the average activity at 20, 40 and 60 min
45 and the corresponding turnover frequency (TOF) was calculated to obtain the intrinsic activity
46 for further comparison among the above four configurations. As shown in Table 1, both the Pt
47 NCs/α-Fe₂O₃ NSs and Pt NCs/α-Fe₂O₃ Rhomb exhibit higher specific rate and TOF relative to
48 the other two α-Fe₂O₃ supported Pt NPs catalysts following the order of Pt NCs/α-Fe₂O₃ Rhomb
49
50
51
52
53
54
55
56
57
58
59
60

1
2
3 > Pt NCs/ α -Fe₂O₃ NSs > Pt NPs/ α -Fe₂O₃ NSs > Pt NPs/ α -Fe₂O₃ Rhomb. In particular, the
4 combination of Pt NCs and α -Fe₂O₃ Rhomb possesses nearly 20 times higher specific rate than
5 Pt NPs/ α -Fe₂O₃ Rhomb catalyst. What is noteworthy is that the Pt NCs enclosed by Pt {100}
6 facet is speculated to be the more ideal pair of α -Fe₂O₃ Rhomb rather than α -Fe₂O₃ NSs. On the
7 contrary, the α -Fe₂O₃ NSs could be regarded as the more suitable configuration with Pt NPs
8 regarding the performance.
9

10
11
12 **2.3. DFT Calculation for Understanding of Relation between Catalytic Activity and**
13 **Catalysts Surface Properties.** In fact, the great difference among these catalysts is mainly
14 originated from the various exposed facet matching between supported Pt clusters and α -Fe₂O₃,
15 which offers different active sites towards CO and O₂ thus in turn acts on the adsorption nature
16 of the overall catalysts. To reveal the essence of the distinct activity shown by the four-targeted
17 catalysts, DFT calculations were performed. Adsorption energy for CO and O₂ on four
18 configurations including Pt {111}/Fe₂O₃ {001}, Pt {111}/Fe₂O₃ {104}, Pt {100}/Fe₂O₃ {001}
19 and Pt {100}/Fe₂O₃ {104} are determined (Figure 3a). For each slab with adsorbate, various
20 possible adsorption sites were studied in this work, containing top, bridge, hollow on Pt clusters,
21 and top of Fe around Pt cluster as well (Figure S6). As for CO molecule, the adsorption energy
22 can be written as:
23
24
25
26
27
28
29
30
31
32
33
34
35
36
37
38
39
40
41

$$E_{ads(CO)} = E_{S-CO} - E_S - E_{CO} \quad (1)$$

42 where $E_{ads(CO)}$ is the adsorption energy of CO molecule; E_{S-CO} is the energy of the catalyst slab
43 with the adsorbate on surface; E_S is the energy of the catalyst slab without the adsorbate and E_{CO}
44 is the energy of dissociative CO molecule in gas phase. The adsorption energy for O₂ is
45 determined in a similar way (see the details in the supporting information). Table S1-4 show the
46 corresponding adsorption energy on each adsorption site. The adsorption energy on pure Pt
47
48
49
50
51
52
53
54
55
56
57
58
59
60

1
2
3 (111), Pt (100), Fe₂O₃ (001) and Fe₂O₃ (104) (Table S5) were collected and calculated for
4
5 reference. The more negative calculated adsorption energy of CO on the Pt surface than α -Fe₂O₃
6
7 support and opposite trend towards O₂ adsorption indicates that CO is prone to preferentially
8
9 adsorb on noble Pt clusters but α -Fe₂O₃ support is in the favor of O₂ adsorption. In terms of the
10
11 Pt {111}/Fe₂O₃ {104} catalyst, the calculated stable adsorption energy towards CO and O₂ are -
12
13 2.003 eV per CO molecule on Pt surface and -1.599 eV per O₂ molecule on Fe₂O₃ support which
14
15 owns the most negative adsorption energy of CO and the largest adsorption energy difference
16
17 between CO and O₂ by 0.404 eV among all the four cases (Figure 3a), resulting in the strong
18
19 adsorption of CO on Pt {111} almost catching up with pure Pt (111) (-2.09 eV) (Table S5). As a
20
21 result, more active sites on Pt {111} could be easily occupied by CO and simultaneously further
22
23 leads to the poisoning of catalysts.⁹ Therefore, the reason for sluggish efficiency of CO
24
25 conversion under low temperature range when the reaction is catalyzed by the Pt NPs/ α -Fe₂O₃
26
27 Rhomb catalysts can be well explained. When the supported Pt NPs was taken place by Pt NCs
28
29 with enclosed planes of Pt {100}, the CO adsorption on Pt surface weakened along with the
30
31 stronger adsorption of O₂ on α -Fe₂O₃ Rhomb support and the energy difference (ΔE_{ads}) between
32
33 $E_{ads(CO)}$ and $E_{ads(O_2)}$ obviously decreased, indicating that the activation of O₂ became facilitated
34
35 thus the effect of CO poisoning occurring at low temperature on the surface is successfully
36
37 eliminated which coincides well with the experimental results. For the other two cases of Pt
38
39 {111}/Fe₂O₃ {001} and Pt {100}/Fe₂O₃ {001}, even though both the adsorption of CO on Pt
40
41 surface weakened compared to the Pt {111}/Fe₂O₃ {104}, the number of activated O atoms on
42
43 the Fe₂O₃ {001} also decreased due to the concurrently weak adsorption towards O₂ on Fe₂O₃
44
45 {001} surface so the ex-situ catalytic activity for CO oxidation of Pt NPs/ α -Fe₂O₃ NSs and Pt
46
47 NCs/ α -Fe₂O₃ NSs are still not in excess of Pt NCs/ α -Fe₂O₃ Rhomb. The combination of Pt
48
49
50
51
52
53
54
55
56
57
58
59
60

1
2
3 {100}/Fe₂O₃ {104}, therefore constructed relatively optimal adsorption configuration with the
4 preferential adsorption of O₂ (-1.612 eV), and proper CO adsorption energy (-1.790 eV) making
5 more sites active towards CO oxidation.
6
7
8

9
10 The adsorption and activation of O₂ is a key step during the CO oxidation process so the
11 modification of materials surface property to supply sufficient active sites and facilitating the
12 dissociated adsorption of O₂ turn to be especially critical. In order to further explore the facet-
13 dependent SMSI between supported Pt cluster and α -Fe₂O₃ together with the intrinsic
14 modification of surface adsorption, the d-band density of states (DOS) about Pt and surface Fe in
15 Fe₂O₃ relative to the Fermi level has been calculated to study the strong orbital hybridizations.
16 All the d-band DOS of Pt {111}, Pt {100}, Fe in α -Fe₂O₃ {001}, {104} surface before and after
17 matching were shown in Figure S7. It could be clearly seen that there exists obvious distribution
18 difference of DOS originated from the occupancy of their d-bands under all the above cases,
19 which indicates the strong interaction between α -Fe₂O₃ support and Pt clusters with specific
20 enclosed facets. In addition, the adsorption property is generally closely related to the d-band
21 center of transition metal. After interacting with the d-band electrons of a transition metal
22 surface, the local density of states at the adsorbate will split off to bonding and anti-bonding.
23 When the d-band center of transition metal surface moves down which means the Fermi level
24 relatively shifts up, the number of empty anti-bonding decreases thus the bond between
25 adsorbate and metal surface becomes weaker and vice versa.²⁸ The d-band center of Fe in pure α -
26 Fe₂O₃ support and after matching with Pt {111} and Pt {100} are calculated to explain the
27 characteristic adsorption towards O₂ among the studied four cases (Figure S8). It shows that the
28 d-band center of Fe in α -Fe₂O₃ {104} gives rise to down-shift after loading either Pt {100} or Pt
29 {111} but the former forms stronger bonding owing to the relatively upper position of Fe d-band
30
31
32
33
34
35
36
37
38
39
40
41
42
43
44
45
46
47
48
49
50
51
52
53
54
55
56
57
58
59
60

center that agrees with the calculated adsorption energy. Similar trends can be also found for the α -Fe₂O₃ {001} cases. In order to figure out the origin of the catalytic cycle of CO oxidation, the Gibbs energy, ΔG , was determined to reflect the ease or complexity of the overall reaction for different Pt/ α -Fe₂O₃ catalysts. Based on the model mentioned in the Scheme 1, the Gibbs energy of the reaction path can be defined as:

$$\Delta G = E_{S-CO} + E_{S-O_2} - E_S - E_{CO_2} - E_{S-O} \quad (2)$$

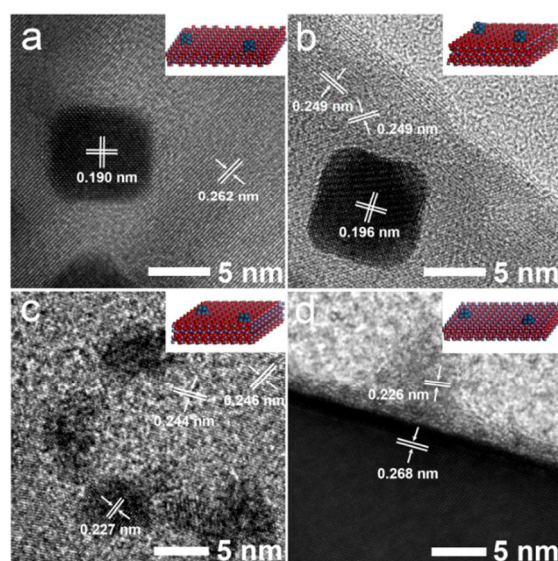
where E_{S-CO} is the stable energy of the catalyst slab with CO adsorbed; E_{S-O_2} is that with O₂ adsorbed; E_S is the energy of the catalyst slab without any adsorbate; E_{CO_2} is the stable energy of dissociated CO₂ molecule and E_{S-O} is the energy of the slab with an adsorbed O atom. ΔG as described in Equation (2) on the four different catalysts is shown in Figure S9 and Table S6 are -6.665 eV, -6.539 eV, -6.039 eV and -5.528 eV which is corresponding to catalyst configurations for Pt {100}/Fe₂O₃ {104}, Pt {100}/Fe₂O₃ {001}, Pt {111}/Fe₂O₃ {001} and Pt {111}/Fe₂O₃ {104}, respectively. Distinctly, the calculated ΔG for CO oxidation on Pt {100}/Fe₂O₃ {104} surface is the most negative, indicating a larger thermodynamic driving force for the reaction, which is in agreement with the lowest T₁₀₀ of Pt {100}/Fe₂O₃ {104} among the four catalysts. Figure 3b shows the fitting linear curve between ΔG and T₁₀₀, highly coinciding with the experimental results as well.

3. CONCLUSIONS

In summary, we raise a novel and rational design approach for efficient catalysts towards CO oxidation reaction. We demonstrate that the modification of overall adsorption property by controlling the exposed facets matching configuration of both noble metal clusters and oxides supports has great influence on the catalytic activity. From the DFT calculations, the intrinsic origin of facet matching-dependent adsorption was well explained. Optimal occupation of the

1
2
3 active sites by CO and O₂ could further promote the potential performance. Based on the studied
4
5 four kinds of catalysts, the activity towards CO oxidation following the order of Pt {100}/Fe₂O₃
6
7 {104} > Pt {100}/Fe₂O₃ {001} > Pt {111}/Fe₂O₃ {001} > Pt {111}/Fe₂O₃ {104} well proved
8
9 that the weakened CO adsorption and feasible O₂ activation hindered the poisoning to catalysts at
10
11 low temperature thus enhanced the reaction efficiency. Above all, it provides an applicable path
12
13 for determining the catalytic performance via appropriate engineering of interface interaction.
14
15

16 17 18 FIGURES



44
45 **Figure 1.** High-resolution TEM micrographs of different facet matching Pt/ α -Fe₂O₃ catalysts:
46
47 (a) Pt {100}/Fe₂O₃ {104}, (b) Pt {100}/Fe₂O₃ {001}, (c) Pt {111}/Fe₂O₃ {001}, (d) Pt
48
49 {111}/Fe₂O₃ {104}. The insets are the corresponding atomic model illustrations.
50

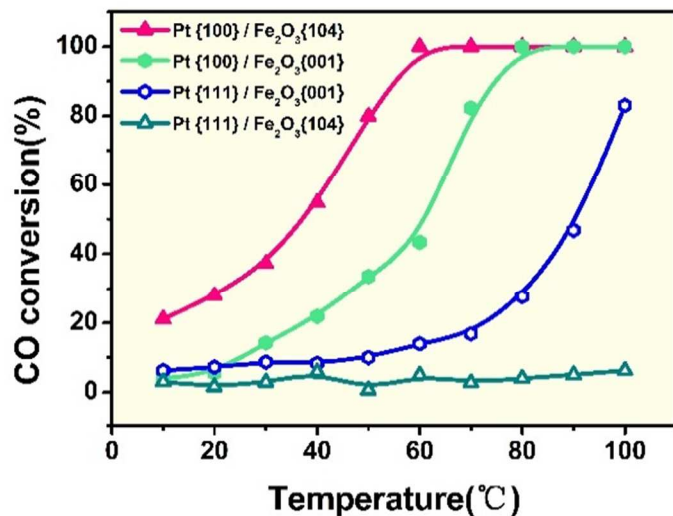


Figure 2. Comparison of CO conversion curves for CO oxidation as a function of temperature on different facets matching catalysts: Pt NC/Fe₂O₃ Rhomb: Pt {100}/Fe₂O₃ {104}, Pt NC/Fe₂O₃ NS: Pt {100}/Fe₂O₃ {001}, Pt NP/Fe₂O₃ NS: Pt {111}/Fe₂O₃ {001} and Pt NP/Fe₂O₃ Rhomb: Pt {111}/Fe₂O₃ {104}. Conditions: 1 vol % CO, 1 vol % O₂, 98 vol % N₂, space velocity (SV) = 18, 750 mL·h⁻¹·g⁻¹_{catalyst}.

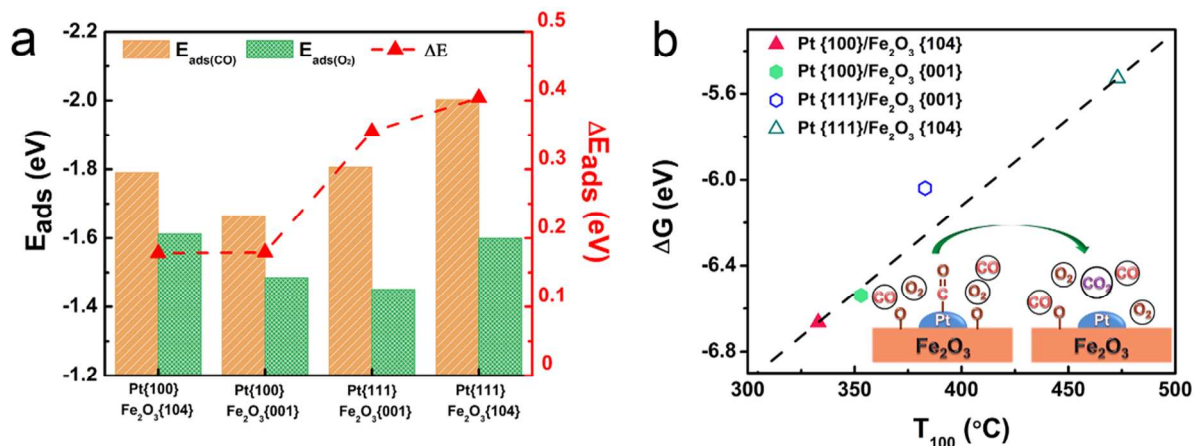
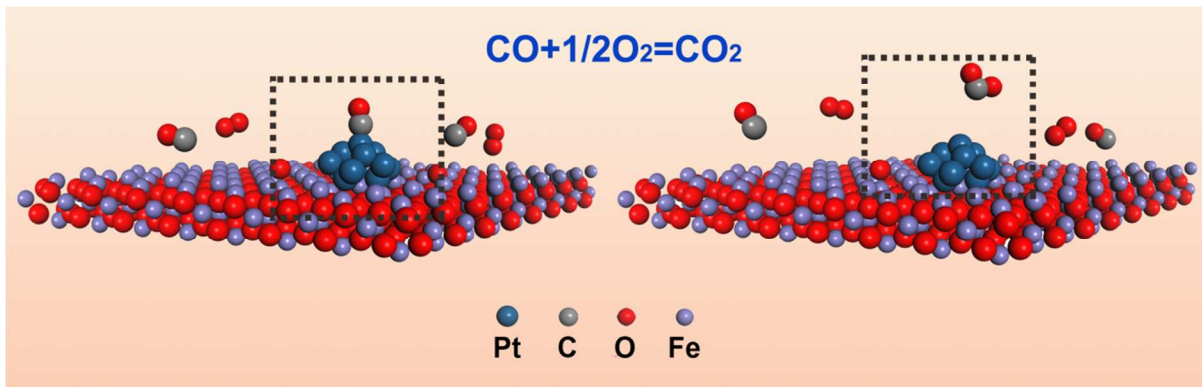


Figure 3. (a) Calculated stable adsorption energy for CO ($E_{ads(CO)}$), O₂ ($E_{ads(O_2)}$), and the energy difference ΔE_{ads} between $E_{ads(CO)}$ and $E_{ads(O_2)}$, ΔE_{ads} , on Pt {100}/Fe₂O₃ {104}, Pt {100}/Fe₂O₃ {001}, Pt {111}/Fe₂O₃ {001}, Pt {111}/Fe₂O₃ {104}; (b) Fitting linear curve between ΔG (the Gibbs energy) and T_{100} . The inset shows the non-competitive Langmuir-Hinshelwood (L-H) mechanism of CO oxidation.

SCHEMES

Scheme 1. Schematic illustration of CO oxidation reaction process over Pt/Fe₂O₃ catalyst^a



^aThe inset indicates the states of gaseous molecules nearby catalyst before and after CO oxidation reaction.

TABLES.

Table 1. Comparison of specific rates and TOFs of different facet matching Pt/ α -Fe₂O₃ catalysts at 60 °C.

Samples	Pt loading wt%	d _{Pt} (nm)	specific rate, mmol CO h ⁻¹ g _{Pt} ⁻¹	TOF × 10 ² , s ⁻¹
Pt{100}/Fe ₂ O ₃ {104}	5.49	6.2	152.5	5.69
Pt{100}/Fe ₂ O ₃ {001}	5.11	5.6	71.1	2.40
Pt{111}/Fe ₂ O ₃ {001}	5.98	3.7	19.5	0.43
Pt{111}/Fe ₂ O ₃ {104}	5.20	3.6	7.9	0.17

ASSOCIATED CONTENT

Supporting Information. Experimental details including chemicals and materials; synthetic method; structure and composition characterization; measurement of catalytic activity and TOF measurements and calculation method; brief description of computational method used in this study; SEM images; low-magnification TEM images; particle size distribution; PXRD; calculation model of adsorption sites; projected density of states; the calculated d-band center of Fe; the calculated Gibbs energy of CO oxidation; detailed adsorption energy table of CO and O₂ molecules; the calculated Gibbs energy table of CO oxidation. This material is available free of charge via the Internet at <http://pubs.acs.org>.

AUTHOR INFORMATION

Corresponding Author

*Email for J. B. Wu: jianbowu@sjtu.edu.cn

*Email for H. Zhu: hong.zhu@sjtu.edu.cn

*Email for B. L. Lv: lbl604@sxicc.ac.cn

*Email for R. Huang: rhuang@ee.ecnu.edu.cn

Author Contributions

The manuscript was written through contributions of all authors. All authors have given approval to the final version of the manuscript. ‡These authors contributed equally.

Funding Sources

National Key R&D Program of China, 2017YFB0406000;

1
2
3 The National Science Foundation of China, 51521004;
4

5 The National Science Foundation of China, 51420105009;
6

7
8 The Shanghai Sailing Program, 16YF1406000;
9

10 The Youth Innovation Promotion Association of CAS, 2015141.
11

12 13 ACKNOWLEDGMENT 14

15
16 The work is sponsored by the thousand talents program for distinguished young scholars from
17 Chinese government, National Key R&D Program of China (No. 2017YFB0406000), and the
18 National Science Foundation of China (51521004 and 51420105009), and start-up fund (J.B.W.)
19 and the Zhi-Yuan Endowed fund (T.D.) from Shanghai Jiao Tong University. H.Z. thanks the
20 financial support from the Shanghai Sailing Program (16YF1406000) and the computing
21 resources from Shanghai Jiao Tong University Supercomputer Center. B.L.L. thanks the support
22 from Youth Innovation Promotion Association of Chinese Academy of Sciences (2015141). The
23 authors thank Instrumental Analysis Center of Shanghai Jiao Tong University for access to SEM.
24 The authors also thank State Key Laboratory of Metal Matrix Composites for access to TEM.
25
26
27
28
29
30
31
32
33
34
35
36
37

38 ABBREVIATIONS 39

40 SMSI, The Strong Metal-Support Interaction; NPs, nanoparticles; L-H, Langmuir-Hinshelwood;
41 NCs, nanocubes; NSs, nanosheets; Rhomb, rhombohedra; DFT, density functional theory; SEM,
42 scanning electron microscope; OAm, oleylamine; TEM, transition electron microscope; PXRD,
43 powder X-ray diffraction; fcc, face-centered cubic; SV, space velocity; T_{100} , 100% efficiency of
44 CO conversion; TOF, turnover frequency; DOS, density of states; ΔG , the Gibbs energy.
45
46
47
48
49
50
51
52
53
54
55
56
57
58
59
60

REFERENCES

- (1) Zhao, K.; Tang, H.; Qiao, B.; Li, L.; Wang, J. High Activity of Au/ γ -Fe₂O₃ for CO Oxidation: Effect of Support Crystal Phase in Catalyst Design. *ACS Catal.* **2015**, *5*, 3528-3539.
- (2) Corma, A.; Serna, P. Chemoselective Hydrogenation of Nitro Compounds with Supported Gold Catalysts. *Science* **2006**, *313*, 332-334.
- (3) Lanzafame, P.; Centi, G.; Perathoner, S. Catalysis for Biomass and CO₂ Use through Solar Energy: Opening New Scenarios for a Sustainable and Low-Carbon Chemical Production. *Chem. Soc. Rev.* **2014**, *43*, 7562-7580.
- (4) Zhou, Y.; Doronkin, D. E.; Chen, M.; Wei, S.; Grunwaldt, J. D. Interplay of Pt and Crystal Facets of TiO₂: CO Oxidation Activity and Operando XAS/DRIFTS Studies. *ACS Catal.* **2016**, *6*, 7799-7809.
- (5) Campbell, C. T. Catalyst-Support Interactions: Electronic Perturbations. *Nat. Chem.* **2012**, *4*, 597-598.
- (6) Haller, G. L.; Resasco, D. E. Metal-Support Interaction: Group VIII Metals and Reducible Oxides. *Adv. Catal.* **1989**, *36*, 173-235.
- (7) Gatla, S.; Aubert, D.; Agostini, G.; Mathon, O.; Pascarelli, S.; Lunkenbein, T.; Willinger, M. G.; Kaper, H. Room-Temperature CO Oxidation Catalyst: Low-Temperature Metal-Support Interaction between Platinum Nanoparticles and Nanosized Ceria. *ACS Catal.* **2016**, *6*, 6151-6155.
- (8) Ahmadi, M.; Mistry, H.; Roldan Cuenya, B. Tailoring the Catalytic Properties of Metal Nanoparticles via Support Interactions. *J. Phys. Chem. Lett.* **2016**, *7*, 3519-3533.

1
2
3 (9) Liu, K.; Wang, A.; Zhang, T. Recent Advances in Preferential Oxidation of CO Reaction
4 over Platinum Group Metal Catalysts. *ACS Catal.* **2012**, *2*, 1165-1178.
5
6

7
8 (10) Korotkikh, O.; Farrauto, R. Selective Catalytic Oxidation of CO in H₂: Fuel Cell
9 Applications. *Catal. Today* **2000**, *62*, 249-254.
10
11

12
13 (11) Huang, Y.; Wang, A.; Li, L.; Wang, X.; Su, D.; Zhang, T. "Ir-in-Ceria": A Highly
14 Selective Catalyst for Preferential CO Oxidation. *J. Catal.* **2008**, *255*, 144-152.
15
16

17
18 (12) Norskov, J. K.; Bligaard, T.; Rossmeisl, J.; Christensen, C. H. Towards the Computational
19 Design of Solid Catalysts. *Nat. Chem.* **2009**, *1*, 37-46.
20
21

22
23 (13) Newton, M. A.; Van, B. W. Combining Synchrotron-Based X-Ray Techniques with
24 Vibrational Spectroscopies for the In Situ Study of Heterogeneous Catalysts: a View from a
25 Bridge. *Chem. Soc. Rev.* **2010**, *39*, 4845.
26
27

28
29 (14) Topsøe, H. Developments in Operando Studies and In Situ Characterization of
30 Heterogeneous Catalysts. *J. Catal.* **2003**, *216*, 155-164.
31
32

33
34 (15) Tao, F. F.; Salmeron, M. In Situ Studies of Chemistry and Structure of Materials in
35 Reactive Environments. *Science* **2011**, *331*, 171-174.
36
37

38
39 (16) Alayon, E. M. C.; Singh, J.; Nachtegaal, M.; Harfouche, M.; van Bokhoven, J. A. On
40 Highly Active Partially Oxidized Platinum in Carbon Monoxide Oxidation over Supported
41 Platinum Catalysts. *J. Catal.* **2009**, *263*, 228-238.
42
43

44
45 (17) Qiao, B.; Lin, J.; Wang, A.; Chen, Y.; Zhang, T.; Liu, J. Highly Active Au₁/Co₃O₄ Single-
46 Atom Catalyst for CO Oxidation at Room Temperature. *Chin. J. Catal.* **2015**, *36*, 1505-1511.
47
48
49
50

1
2
3 (18) Lin, J.; Wang, A.; Qiao, B.; Liu, X.; Yang, X.; Wang, X.; Liang, J.; Li, J.; Liu, J.; Zhang,
4 T. Remarkable Performance of Ir₁/FeO_x Single-Atom Catalyst in Water Gas Shift Reaction. *J.*
5
6
7
8 *Am. Chem. Soc.* **2013**, *135*, 15314-15317.

9
10
11 (19) Wei, H.; Liu, X.; Wang, A.; Zhang, L.; Qiao, B.; Yang, X.; Huang, Y.; Miao, S.; Liu, J.;
12 Zhang, T. FeO_x-Supported Platinum Single-Atom and Pseudo-Single-Atom Catalysts for
13
14
15
16
17
18
19
20
21
22
23
24
25
26
27
28
29
30
31
32
33
34
35
36
37
38
39
40
41
42
43
44
45
46
47
48
49
50
51
52
53
54
55
56
57
58
59
60

Chemoselective Hydrogenation of Functionalized Nitroarenes. *Nat. Commun.* **2014**, *5*, 5634.

(20) Jiang, Z.; Yang, Y.; Shangguan, W.; Jiang, Z. Influence of Support and Metal Precursor
on the State and CO Catalytic Oxidation Activity of Platinum Supported on TiO₂. *J. Phys. Chem.*
C **2012**, *116*, 19396-19404.

(21) Kozlov, S. M.; Neyman, K. M. Effects of Electron Transfer in Model Catalysts Composed
of Pt Nanoparticles on CeO₂ (1 1 1) Surface. *J. Catal.* **2016**, *344*, 507-514.

(22) Yang, H. G.; Sun, C. H.; Qiao, S. Z.; Zou, J.; Liu, G.; Smith, S. C.; Cheng, H. M.; Lu, G.
Q. Anatase TiO₂ Single Crystals with a Large Percentage of Reactive Facets. *Nature* **2008**, *453*,
638-641.

(23) Pan, J.; Liu, G.; Lu, G. Q.; Cheng, H. M. On the True Photoreactivity Order of {001},
{010}, and {101} Facets of Anatase TiO₂ Crystals[†]. *Angew. Chem. Int. Ed.* **2011**, *50*, 2133-2137.

(24) Si, R.; Flytzani-Stephanopoulos, M. Shape and Crystal-Plane Effects of Nanoscale Ceria
on the Activity of Au-CeO₂ Catalysts for the Water-Gas Shift Reaction. *Angew. Chem.*
Int. Ed. **2008**, *47*, 2884-2887.

1
2
3 (25) Allian, A. D.; Takanabe, K.; Furdala, K. L.; Hao, X.; Truex, T. J.; Cai, J.; Buda, C.;
4 Neurock, M.; Iglesia, E. Chemisorption of CO and Mechanism of CO Oxidation on Supported
5 Platinum Nanoclusters. *J. Am. Chem. Soc.* **2011**, *133*, 4498-4517.
6
7

8
9
10 (26) Schubert, M. M.; Hackenberg, S.; van Veen, A. C.; Muhler, M.; Plzak, V.; Behm, R. J.
11 CO Oxidation over Supported Gold Catalysts-"Inert" and "Active" Support Materials and Their
12 Role for the Oxygen Supply during Reaction. *J. Catal.* **2001**, *197*, 113-122.
13
14
15

16 (27) Kotobuki, M.; Watanabe, A.; Uchida, H.; Yamashita, H.; Watanabe, M. Reaction
17 Mechanism of Preferential Oxidation of Carbon Monoxide on Pt, Fe, and Pt-Fe/Mordenite
18 Catalysts. *J. Catal.* **2005**, *236*, 262-269.
19
20
21
22

23 (28) Hammer, B.; Nørskov, J. K. Theoretical Surface Science and Catalysis-Calculations and
24 Concepts. *Adv. Catal.* **2000**, *31*, 71-129.
25
26
27
28

29 (29) Fu, Q.; Li, W. X.; Yao, Y.; Liu, H.; Su, H. Y.; Ma, D.; Gu, X. K.; Chen, L.; Wang, Z.;
30 Zhang, H. Interface-Confined Ferrous Centers for Catalytic Oxidation. *Science* **2010**, *328*, 1141-
31 1144.
32
33
34
35
36
37

38 (30) Tsao, K. C.; Yang, H. Continuous Production of Carbon-Supported Cubic and Octahedral
39 Platinum-Based Catalysts Using Conveyor Transport System. *Small* **2016**, *12*, 4808-4814.
40
41
42
43

44 (31) Ma, Y.; Gao, W.; Shan, H.; Chen, W.; Shang, W.; Tao, P.; Song, C.; Addiego, C.; Deng,
45 T.; Pan, X.; Wu, J. Platinum-Based Nanowires as Active Catalysts toward Oxygen Reduction
46 Reaction: In Situ Observation of Surface-Diffusion-Assisted, Solid-State Oriented Attachment.
47 *Adv. Mater.* **2017**, *29*, 1703460.
48
49
50
51
52
53
54
55
56
57
58
59
60

(32) Zhang, C.; Sang, Y. H.; Trout, A.; Peng, Z. Solid-State Chemistry-Enabled Scalable Production of Octahedral Pt-Ni Alloy Electrocatalyst for Oxygen Reduction Reaction. *J. Am. Chem. Soc.* **2014**, *136*, 7805-7808.

(33) Chen, L.; Yang, X.; Chen, J.; Liu, J.; Wu, H.; Zhan, H.; Liang, C.; Wu, M. Continuous Shape- and Spectroscopy-Tuning of Hematite Nanocrystals. *Inorg. Chem.* **2010**, *49*, 8411-8420.

(34) Wang, C.; Shi, J.; Cui, X.; Zhang, J.; Zhang, C.; Wang, L.; Lv, B. The Role of CO₂ in Dehydrogenation of Ethylbenzene over Pure α -Fe₂O₃ Catalysts with Different Facets. *J. Catal.* **2017**, *345*, 104-112.

(35) Liu, X.; Korotkikh, O.; Farrauto, R. Selective Catalytic Oxidation of CO in H₂: Structural Study of Fe Oxide-Promoted Pt/Alumina Catalyst. *Appl. Catal. A* **2002**, *226*, 293-303.

(36) An, K.; Alayoglu, S.; Musselwhite, N.; Plamthottam, S.; Melaet, G.; Lindeman, A. E.; Somorjai, G. A. Enhanced CO oxidation Rates at the Interface of Mesoporous Oxides and Pt Nanoparticles. *J. Am. Chem. Soc.* **2013**, *135*, 16689-16696.

SYNOPSIS

